Pergamon

Cement and Concrete Research, Vol. 25, No. 3, pp. 605-616, 1995

0008-8846/95 $9.50+.00

0008-8846(95)00049-6

AUTOMATED CRACK IDENTIFICATION FOR CEMENT PASTE

David Darwin, Mohamed Nagib Abou-Zeid, and Kirk W. Ketcham,*
Structural Engineering and Materials Laboratory
2006 Learned Hall, University of Kansas
Lawrence, Kansas 66045

(Refereed)
(Received May 16, 1994; in final form February 21, 1995)

ABSTRACT

The development of an automated procedure for the identification of microcracks in cement paste using backscattered electron images of polished epoxy-impregnated specimens is described. Digitized images are acquired using an integrated scanning electron microscope/image acquisition system. Cracks are identified based on local changes in image intensity (gray level) and feature geometry. The gray level of epoxy-filled cracks is affected by the density of underlying and adjacent phases. As a result, cracks cannot be identified based on gray level alone. Combined procedures that establish the floor of the crack, a minimum gradient in the gray level adjacent to cracks, and minimum differences in gray level between the floor of a crack and adjacent solid phases provide a reproducible and consistent technique for crack identification in cement paste. The crack patterns observed using these procedures show that the denser phases within hydrated cement paste exhibited lower crack density than phases with lower density and that a significant portion of the cracking occurs through the softest phase, undesignated product (UDP), and at the boundary between UDP and other phases.

Introduction

The correlation between stress-strain behavior and the increase in microcracking in cementitious materials has been under study at the University of Kansas for nearly 20 years (1-11). Since 1980, the scanning electron microscope (SEM) has been used with secondary electron (SE) imaging (3, 5, 6) and, more recently, backscattered electron (BSE) imaging (9-11) to identify and measure the microcracks. The statistical scatter in the crack patterns requires relatively large areas to be surveyed. In the early work, the cracks were identified by eye and measured manually on the SEM screen (3, 5, 6). This procedure is by nature subjective, and operator fatigue can reduce objectivity (10). Therefore, for several years, a principal goal of the research effort has been to automate the crack identification and measuring process, a process that includes the segmentation (marking) of the cracks so that the geometric properties and microstructural position can be recorded.

* Current Address: Black & Veatch, PO Box 8405, Kansas City, MO 64114

BSE images of polished epoxy-impregnated specimens allow individual phases to be identified based on relative intensity (12-18) – high density phases, like unhydrated cement particles, are bright, while low density epoxy-filled cracks and voids are dark. Differences in intensity, along with apparent geometric properties, allow the human eye and brain to distinguish cracks from other features. Unfortunately, the translation of this process into computer code is not straightforward. The process is complicated by the fact that the backscattered electron image intensity of low density phases is dependent upon the density of adjacent and underlying phases. This causes the intensity, or gray level, within an individual crack to change as it passes through or adjacent to different phases within hydrated cement paste. Thus, absolute intensity, as measured by the gray scale of a digital image, is insufficient to identify cracks. This causes no problems for the human eye, which largely ignores changes in gray level along the length of a crack and picks out individual features based on local changes in intensity.

The process of developing an automated crack identification procedure first involved the application of standard techniques used in image analysis, such as gradient, edge detection, and a number of other image filters or kerns (19, 20); none of these proved satisfactory for identifying and segmenting cracks.

The next step in the development of an automated procedure involved a study of the nature of the changes in gray level that occur in the vicinity of features that are readily identified as cracks in BSE images. Initial work indicated that differences in gray level between the center of a crack and adjacent regions could be used to identify about 50 percent of the cracks (10). To improve the technique, studies were made of gray level intensity profiles on scan lines at right angles to cracks and voids (the latter because of the similarity in gray level). These detailed comparisons yielded information that could be incorporated into computer code (11).

This paper describes the development of the resulting procedure for automated identification of microcracks in cementitious material. It has been applied to cement pastes with water-cement ratios (w/c) ranging from 0.3 to 0.5, both with and without mineral admixtures. The technique allows cracks with widths as low as 0.1 μm to be identified.

Experimental Work

Materials and Test Specimens

The examples presented in this paper involve backscattered electron images of cement paste with a w/c of 0.5. ASTM Type I portland cement with the following Bogue calculated composition was used: C_3S 60 percent, C_2S 17 percent, C_3A 5.5 percent, and C_4AF 9.3 percent.

Specimens were cast as 25 x 25 x 127 mm prisms and cured for 28 days in lime-saturated water. Some specimens (shortened to 76 mm) were loaded to preselected compressive strains and then unloaded. The numerical results presented in this paper compare the results for a specimen loaded in compression to 6000 με with a companion nonloaded specimen. [Nonloaded specimens serve as controls to account for the effects of specimen preparation, which are assumed to be the same for both loaded and nonloaded specimens.]

After loading, the specimens, along with companion nonloaded specimens, were sectioned into transversely and longitudinally oriented 1 mm wafers using a low-speed diamond saw. The wafers were placed in a sonicator bath containing ethanol for two minutes and then placed in an oven at 105°C for 24 hours, cooled in a dessicator cabinet, and impregnated with ultra low viscosity epoxy within 48 hours of sectioning (11).

Following polymerization of the epoxy, the wafers were cut into four SEM specimens and polished manually with progressively finer grades of silicon carbide paper and diamond paste. Final polishing was completed using 0.5 μm diamond paste. Prior to viewing in the SEM, specimens were coated with a 20 nm layer of gold palladium.

Image Acquisition

The cement paste specimens were studied using a Philips 515 scanning electron microscope fitted with a backscattered electron detector consisting of four tilted solid-state detectors on a swing-away arm. The image acquisition system (IAS) consisted of an ELMDAS microcomputer-SEM interface installed in a 486/66 microcomputer.

The SEM parameters used for BSE image acquisition were: accelerating voltage = 25.0 kV, beam current = 0.5 nA, free working distance (FWD) = 25.5 mm, stage tilt = 0°, Wehnelt aperture to filament tip distance = 0.25 mm, and spot size approximately = 100 nm.

The beam current was measured using a Faraday cup and monitored for one hour to insure a stable current. A silicon/magnesium (Si/Mg) standard was used to calibrate the BSE signal on the SEM videoscope, as described by Zhao and Darwin (15, 16). A BSE image of the Si/Mg standard was then acquired using the IAS and compared for signal intensity to an earlier image that served as a standard. Images were acquired in groups of 80, 40 each from two diagonally opposite specimens cut from the original epoxy-impregnated wafers.

The image acquisition system used in this study has the capability of acquiring simultaneous SE and BSE images. The system provides a choice of pixel dwell time (10, 40, 400, or 4,000 μs) and pixel density (1 to 9,999 pixels per scan line and 1 to 9,999 scan lines per image). The pixel dwell time is the time that the electron beam spends on each picture element or pixel. Each pixel corresponds to an individual point on the specimen. The quality of the images is significantly affected by the pixel dwell time – a longer dwell time results in an increase in the total signal for each pixel. Since the signal-to-noise ratio increases with an increase in the signal (21), a longer dwell time results in higher quality images. The image acquisition settings used for this study were: dwell time = 400 μs, pixels per line = 1024, lines per image = 960 (giving 983040 pixels per image at a spacing of 0.077 μm and total image dimensions of 78.85 x 73.92 μm). Total acquisition time per image was 8 min. 19 sec., consisting of 6 min. 35 sec. dwell time and 1 min. 44 sec. computer overhead.

Image acquisition was interrupted every five images to check the beam current, FWD, and calibration of the BSE signal (11, 15, 16). In general, the beam current rarely needed correction, and the FWD needed adjustment only once for each new specimen. The BSE signal required small corrections about once every ten images.

Both TIF and ASCII files were generated for each image. The TIF files were used to display and print the images, while the ASCII files were transferred to a computer workstation for analysis.

Feature Identification

Using BSE imaging, Zhao and Darwin (15-18) identified five phases within the cement paste microstructure on the basis of absolute gray level. From lightest (densest material with the highest backscattered electron coefficient) to the darkest (least dense material with the lowest backscattered electron coefficient), these phases are: 1) unhydrated particles (UH), 2) calcium hydroxide (CH), 3) calcium silicate hydrate within the original boundaries of the cement grains, often referred to as inner product (CSH-IP), 4) the hydration product outside the well-defined phases of UH, CH, and CSH-IP, referred to as undesignated product (UDP) (22), and 5) epoxy-filled voids. With the settings used in this study, the individual phases within UH cannot be distinguished from each other.

There are 256 discrete intensity levels available on an 8 byte graphics card. Based on the settings and calibration used in this study, gray level ranges for the individual phases are: UH 255-215, CH 214-174, CSH-IP 173-144, UDP 143-27, and voids 26-0.

Figs. 1a and 2a are BSE images of cement paste loaded in compression to 0 and 6000 με, respectively.

The current strategy for automated identification of cracks in backscattered electron images of cement paste has evolved as experience was gained in the identification process. The overall procedure first involves the identification of features as potential cracks based on local changes in gray level. The rules used in this step are relatively lenient to insure that the vast majority of the cracks are identified. As a result, some noncrack features are identified as potential cracks. At the same time, some portions of individual cracks are not identified. The next step involves the elimination of the noncrack features and the "recapture" of incorrectly excluded cracks. In the final step, the geometric properties and microstructural positions of the cracks are recorded.

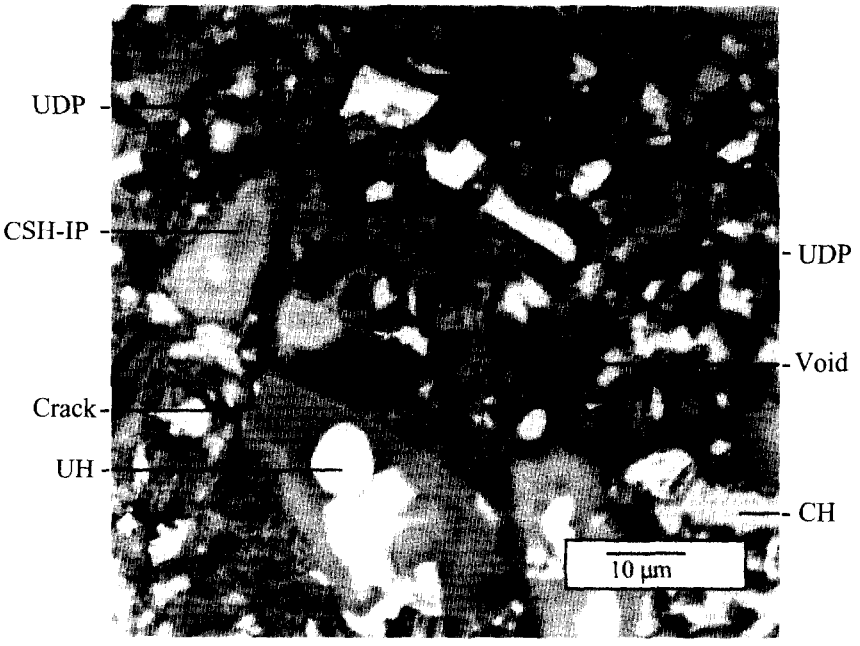

(a)

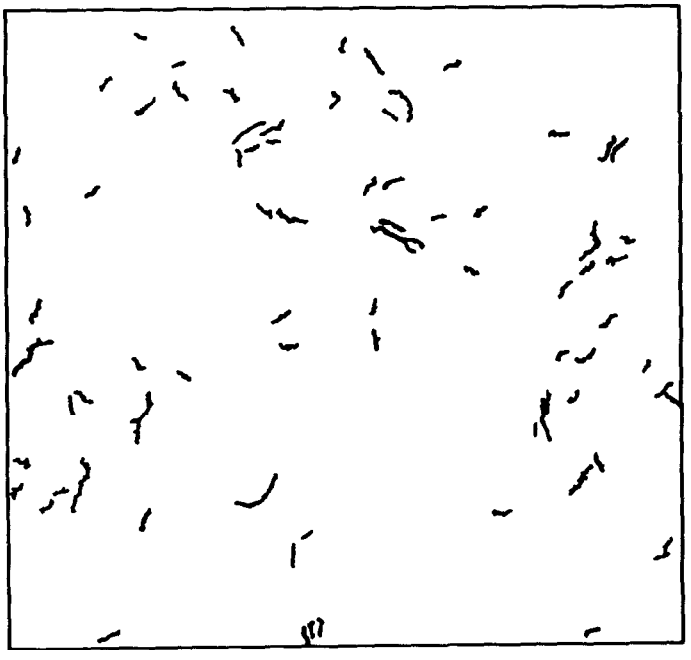

(b)

FIG. 1
(a) BSE Gray Level Image of Nonloaded Cement Paste with w/c = 0.5; age = 28 days
(b) Cracks Identified by Automated Technique

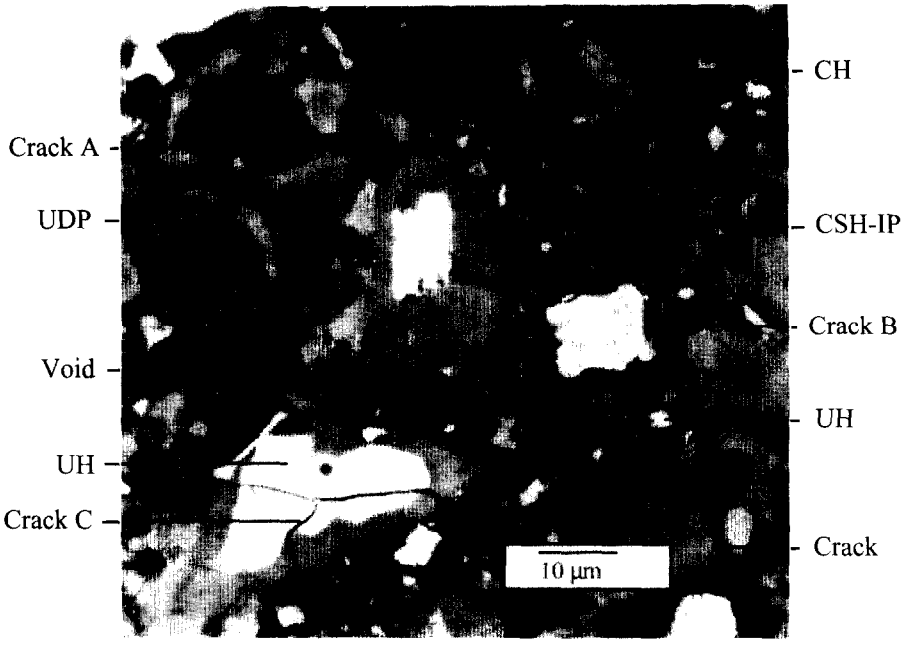

(a)

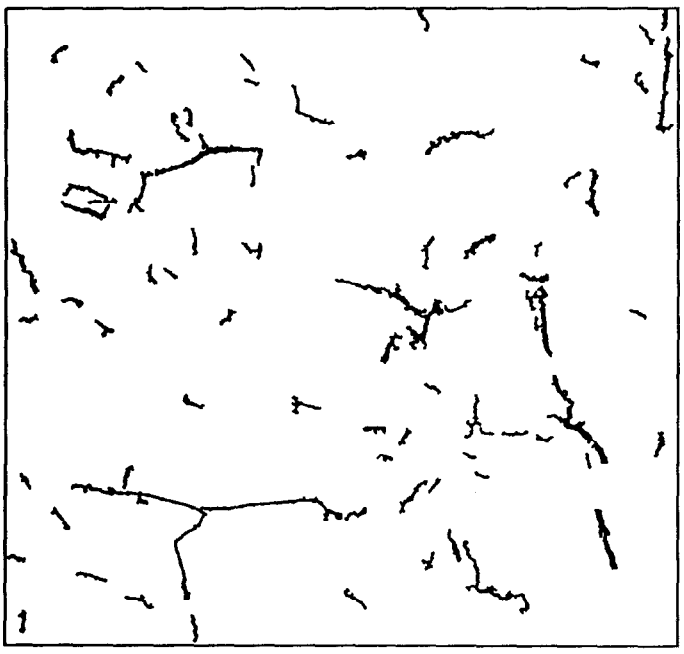

(b)

FIG. 2
(a) BSE Gray Level Image of Cement Paste with w/c = 0.5 loaded to 6000 με; age = 28 days
(b) Cracks Identified by Automated Technique

Identification of Potential Cracks

A study of the changes in pixel intensity on line scans taken perpendicular to cracks in digitized images (such as in Figs. 1a and 2a**) revealed that the gray levels could be represented by three distinct regions, marked Zones A, B, and C in Fig. 3. In Fig. 3, the intensity of individual pixels along the line scan is represented by the vertical axis, and the position of the pixels is represented by the horizontal axis. Zone A represents the crack, initially identified as "the floor of the feature." Zone A is bounded by transition regions, identified as Zone B, that represent the regions over which the intensity of the signal increases, which are, in turn, bounded by regions identified as Zone C (plateau regions) in which the signal intensity is significantly above that of the floor of the feature.

Zone A.–The gray levels within Zone A correlate with the width of the crack. For the settings used in this study, it is observed that scans across cracks that contain at least one pixel with a gray level of 0 exhibit variations in gray level of as much as ± 15 from the mean within Zone A and widths as high as 1.10 μm. Scans across cracks with a minimum gray level greater than 0 exhibit smaller maximum variations in gray level, ± 5, and widths only to 0.27 μm. These observations serve as the principal guidelines in the crack identification process.

Zone B.–As shown in Fig. 3, the floor of the feature is bounded by two transition regions. The rate of change in the gray level within a transition region is greater for cracks than for voids, although there is considerable scatter.

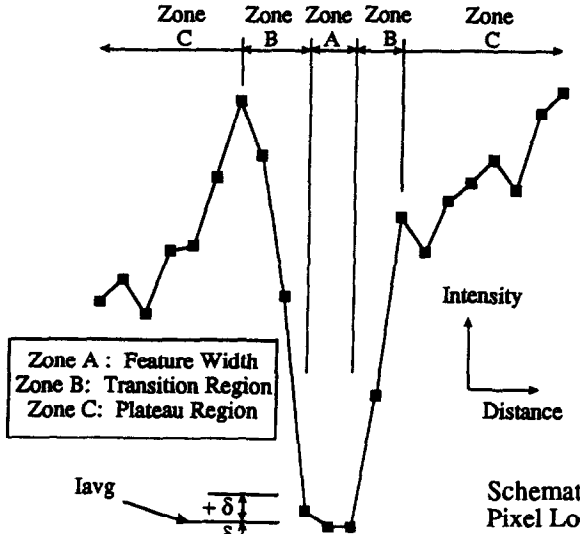

FIG. 3
Schematic of Signal Intensity (gray level) versus Pixel Location along a Scan Line Perpendicular to a Crack

Fig. 4 compares the differences in intensity (I_{dif}) between the average intensity within the floor of a crack (I_{avg}) and the intensity of pixels adjacent to the crack as a function of the distance of the pixels from the edge of the floor of the crack (d_{edge}). To insure that a minimum number of crack features will be misclassified as noncracks, the lower 95 percent confidence limit for I_{dif} is used as the minimum criterion for the increase in gray level within the transition region to identify a feature as a crack. A smoothed version of the lower 95 percent confidence limit for I_{dif} from the edge of the floor of the crack to the end of the transition region (the point at which I_{dif} levels off) is used to define the minimum "slope" of a transition region adjacent to a crack. As shown in Fig. 4,

** Figs. 1a and 2a are selected to illustrate the types of cracks seen in cement paste. The crack density in these micrographs is significantly higher than observed on most polished cement paste specimens in the study.

this locus of points can be represented by a bilinear distribution. For this study, $I_{dif} = 0$ for $d_{edge} \leq 0.112$ μm and $I_{dif} = 158\ d_{edge} - 17.7$ for $0.112\ \mu m \leq d_{edge} \leq 0.27\ \mu m$.

Zone C.–The edge of the plateau (Zone C) is defined as the first pixel with $I_{dif} \geq 25$.

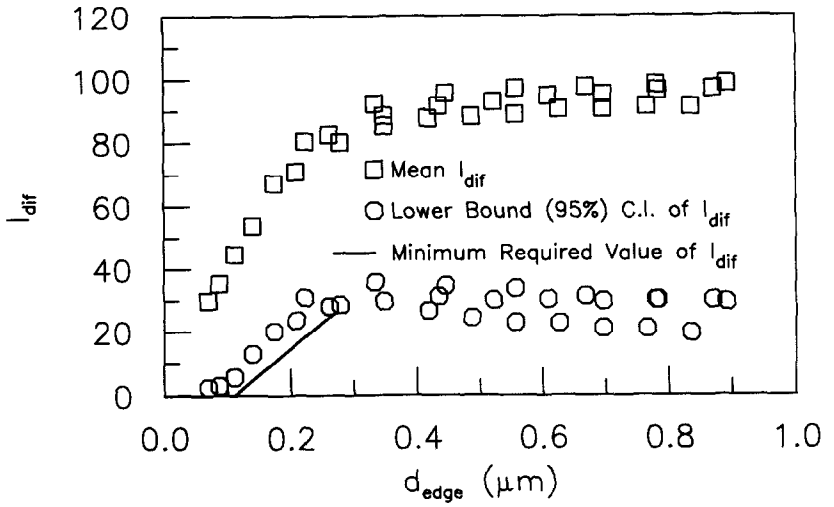

FIG. 4
Mean, Lower 95% Confidence Limit, and Minimum Required Value of Increase in Gray Level in Transition Region (I_{dif}) versus Distance from the Edge of a Crack (d_{edge})

Identification Process.–To initially identify cracks, pixel intensity is evaluated for each pixel within the image. Evaluations are made by scanning in the horizontal, vertical, and two diagonal directions, beginning with the initial pixel in each scan. The running average of the gray level (I_{avg}) is updated as each new pixel is added to the scan, and the first pixel with a gray level outside of the appropriate range (±15 or ±5) defines the previous pixel as the edge of the transition zone. If the requirements described above (for crack width based on minimum gray level and for change in gray level within the transition zones) are met on both sides of the pixel in one of the four scanning directions, the pixel is identified as representing a portion of a crack.

Connecting Adjacent Features

In some instances, the crack identification procedure described above results in the incomplete identification of all pixels within a crack, causing a single crack to appear as two or more shorter cracks.

A technique for connecting these crack segments was developed that picks up most of the missing crack pixels without connecting cracks or other features that should not be connected (11). The technique uses the end pixels (the two pixels within the feature that are the farthest apart, also used to calculate the projected length of the crack) of each initially identified feature: If the distance between end pixels on adjacent features is less than 25 percent of the projected length of the longer feature and the angle formed between the features (defined by the end pixels) is less than 45°, the features are connected on a line between the two closest pixels on the adjacent features. To insure that only crack segments are connected, only features with a minimum area of 0.1 μm^2 and a minimum projected length-to-projected width ratio of 2.25 (geometric properties of observed cracks and crack segments) are connected.

Geometric Properties

The strategy for identifying cracks allows some noncrack features to be retained at this stage

in the process. These noncrack features are typically small voids within UDP or long slender voids, typically adjacent to unhydrated cement grains. A study of the geometric properties of both cracks and noncracks identified specific properties that can be used to separate the two types of features. Two of the criteria used for this purpose are described in the previous paragraph. However, two additional criteria are needed to eliminate the remaining noncrack features. These criteria are based on the area, the projected length, and the ratio of the square of the perimeter to the area of the feature.

1. As illustrated in Fig. 5, for a given perimeter squared-to-area ratio, p^2/A, cracks have higher projected lengths, l_p, than noncracks (Note: l_p for cracks ≥ 1.0 μm). Only features lying below the locus of points represented by

$$\frac{p^2}{A} = 140.5\, l_p \quad \text{for } 1.0\ \mu\text{m} \leq l_p \leq 2.085, \tag{1}$$

and

$$\frac{p^2}{A} = 41.25\, l_p + 85.0 \quad \text{for } 2.085\ \mu\text{m} \leq l_p \leq 6.0\ \mu\text{m} \tag{2}$$

are accepted as cracks. Since no noncrack features (identified based on the gray level criteria) have been observed with a projected length greater than 6 μm, no restrictions are applied to features with projected lengths greater than 6 μm.

2. As illustrated in Fig. 6, small cracks (cross-sectional areas, A, of 1.5 μm^2 or less) exhibit projected lengths above a locus of points represented by

$$l_p = 2.33\, A + 0.90 \tag{3}$$

Features with areas in excess of 1.5 μm^2 are consistently identified correctly based on the transition region requirements and the restrictions illustrated in Fig. 5.

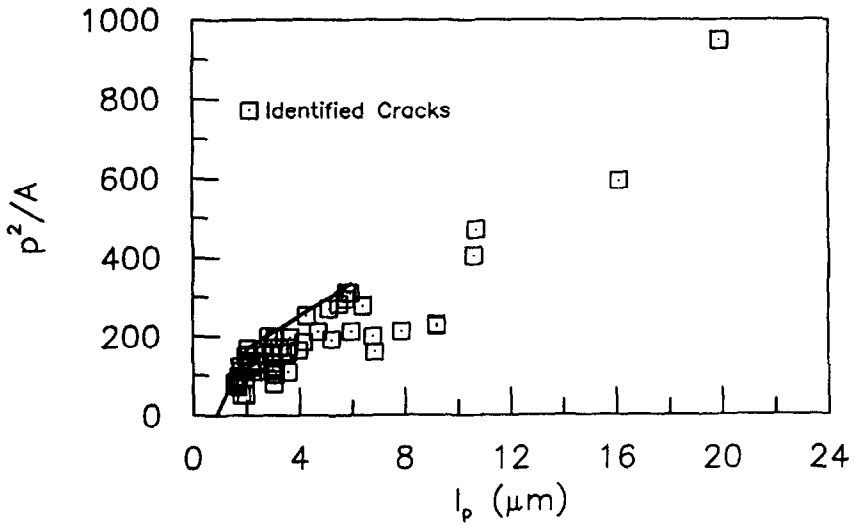

FIG. 5
Perimeter Squared-to-Area Ratio (p^2/A) versus Projected Length (l_p) for Cracks

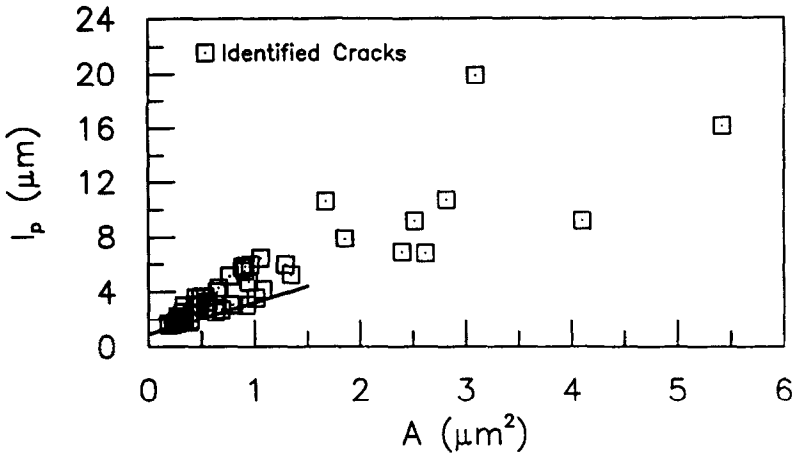

FIG. 6
Projected Length (l_p) versus Area (A) for Cracks

The combined criteria illustrated in Figs. 5 and 6 (Eq. 1-3) serve as the filtering mechanism for separating cracks from noncrack features.

Identification of Phases Adjacent to Cracks

To understand the role played by microcracking in the response of cement paste to stress, it is important to determine what phases or phase boundaries undergo cracking. To do this, a procedure is needed to identify the portions of cracks that pass through phases and along phase boundaries. The proximity of a crack to a phase and the density of the surrounding phases relative to one another are used to determine whether a crack is formed within a single phase or lies on the boundary between two phases.

Phase identification procedures are carried out simultaneously with crack perimeter measurements. As the program progresses from one pixel to another around the perimeter of a crack, it scans in a direction perpendicular to the crack boundary at each pixel to obtain information on the phases adjacent to that pixel. A scan distance of 3.0 μm is used.

Phases are identified using a "smoothed" image, which is obtained by assigning to each pixel the average of its intensity with the intensity of the 8 surrounding pixels. This procedure reduces the effects of noise in the acquired image. A reduction in noise is needed to prevent the erroneous identification of phase boundaries that are, in fact, just adjacent pixels of the same phase that have different intensities due to random variations in the signal. Smoothing is performed only after the cracks have been identified and after the area percent attributed to each phase has been determined. The average intensity assigned to each pixel during this process is based on the original pixel intensities found in the image.

Boundary Cracks

The nature of cracking in hydrated cement paste prevents the direct assignment of a phase to each crack pixel based on the phases immediately in contact with the pixel. The reason for the difficulty is that a crack that is totally immersed in a single phase may closely border a denser phase that has influenced its orientation (see Cracks A and B in Fig. 2a). For this reason, the definition of a boundary crack has been broadened to include, not only cracks that lie immediately on a boundary between two cement paste phases, but also cracks in a softer material that closely parallel the boundary of a denser cement paste phase.

The definition used for a boundary crack requires that an upper limit be established on the proximity of the crack to denser phases. Based on an evaluation of a large number of images, this upper limit is set at 1.5 μm.

Phase Identification Procedure

Phases are evaluated over a distance of 3.0 μm on a line perpendicular to the edge of the crack passing through the center of the current pixel of interest. In the process, the adjacent phases are identified and a determination is made as to whether the crack passes through a single phase or along a phase boundary. The determination of the primary adjacent phase is based on a "phase length," equal to the number of pixels encountered times the distance between adjacent pixels. The primary phase is the phase closest to the perimeter pixel with a phase length ≥ 0.5 μm, the resolution limit for a solid phase in cement paste for the SEM parameters used in this study (21). If the scan produces a phase length < 0.5 μm, the next phase encountered that has a phase length ≥ 0.5 μm is considered to be the primary phase. Scanning continues until a primary phase is found or until 4 phases have been encountered, at which point the phase with the largest phase length becomes the primary phase.

Based on the evaluation of a large number of cracks, specific rules have been established to identify the phases: If a primary phase is encountered on both sides of a crack and the length of this phase is greater than or equal to a required minimum (taken equal to 1.5 μm in the current study), the perimeter pixel in that crack is identified as lying wholly within a single phase. If one primary phase is present on one side of the crack and a different primary phase is present on the other and at least one of these phases has a phase length ≥ 1.5 μm, the pixel is identified as lying on the boundary between the two phases. If the same primary phase is identified on both sides of the crack, but a second, denser phase is encountered within 1.5 μm of the perimeter pixel, the pixel is again identified as lying on the boundary between two phases. The only time that this rule is not used is when denser phases are encountered within 1.5 μm on both sides of the crack. This situation occurs when a soft phase separates two denser phases, with the crack passing through the softer phase. In this case, the perimeter pixel is assigned solely to the softer material.

Results of Analysis

Figs. 1a and 2a are SEM images of cement paste (age = 28 days) loaded to 0 and 6000 με, respectively. Figs. 1b and 2b show the microcracks identified using the procedures described in this paper.

The power of the technique is demonstrated by Crack C in the large unhydrated cement particle in lower left quadrant of Fig. 2a. The gray levels of the pixels within the floor of this crack range from 16 to 128, overlapping the ranges of both voids (0-26) and UDP (27-143). However, based on the crack identification criteria used in the study, the pixels are correctly identified as part of a continuous crack.

Table 1 summarizes the crack analyses of specimens loaded to 0 and 6000 με based on the location of the cracks within microstructure of the cement paste. A maximum crack width criterion of 0.80 μm was used. The total crack densities (expressed here as one-half of the perimeter of the cracks) for the nonloaded and loaded specimens are 50.04 and 79.50 mm/mm^2, respectively. The increase in crack density due to applied compressive strain, 29.46 mm/mm^2, is over 30 times the increase observed for the same applied strain using earlier crack measuring techniques (3, 5, 6).

An understanding of the roles played by the various portions of the microstructure in response to compressive strain can be obtained by comparing the percentage increase in cracking with the area percent of the respective phases.

UDP represents about 46 percent of the total area (and, therefore, volume) of the cement paste. 46 percent of the increase in cracking for an applied strain of 6000 με occurs in this phase. When the associated boundary cracking (UH/UDP = 7.67 percent, CH/UDP = 7.09 percent, and CSH-IP/UDP = 24.34 percent) is added, this value rises to over 85 percent.

CSH-IP occupies about 18 percent of the volume of the paste. However, only about 6 percent of the increase in cracking occurs in this phase. Essentially no increase in cracking occurs at the UH/CSH-IP boundary, while about 4 percent occurs at the boundary with CH.

CH represents about 20 percent of the paste volume. Less than 1 percent of the increase in cracking occurs within this phase, while about 3 percent of the increase occurs at the UH/CH boundary.

UH occupies about 10 percent of the volume and accounts for about 2 percent of the increase in cracking (giving about the same crack density as CH on a per unit volume basis).

TABLE 1
Area Percent, Crack Density* and Change in Crack Density by Phase for Cement Paste with w/c = 0.5; age = 28 days

Phase or Boundary	0 με Area Percent**	0 με Crack Density*** mm/mm²	6000 με Crack Density*** mm/mm²	Change in Crack Density*** mm/mm²
UH	9.96	2.51	3.06	0.55
CH	20.10	4.47	4.65	0.18
CSH-IP	17.52	1.47	3.27	1.80
UDP	45.80	16.27	29.84	13.57
UH/CH		0.79	1.56	0.77
UH/CSH-IP		3.01	2.97	-0.04
UH/UDP		3.67	5.93	2.26
CH/CSH-IP		2.28	3.39	1.11
CH/UDP		8.72	10.81	2.09
CSH-IP/UDP		6.85	14.02	7.17
Voids	5.77			
Cracks	0.85			
Total	100.00	50.04	79.50	29.46

*Based on one-half of the perimeter of features identified as microcracks
**Based on 640 images
***Based on 160 images

The overall picture is one in which the denser phases undergo lower amounts of cracking than the softer phases. The softest phase, UDP, appears to act like a matrix, while the harder phases act like microaggregates. The role of boundary cracking is amply illustrated in Figs. 1a and 2a.

Conclusions

The following conclusions are based on the study of backscattered electron images of cement paste described in this paper:

1. The gray level of epoxy-filled cracks in backscattered electron images of polished cement paste is affected by the density of adjacent and underlying phases. Therefore, cracks cannot be identified based on gray level alone.
2. Epoxy-filled cracks in polished cement paste specimens can be identified based on local changes in gray level and the application of geometric criteria. Combined procedures that establish the floor of the crack, minimum gradient in gray level adjacent to cracks, and minimum differences in gray level between the floor of a crack and adjacent solid phases provide a reproducible and consistent technique for crack identification in cement paste.
3. The denser phases within hydrated cement paste exhibit lower amounts of cracking than phases with lower density. The major portion of the cracking occurs through the softest phase, undesignated product (UDP), and at the boundary between UDP and other phases.

Acknowledgements

The research reported in this paper was sponsored by the Air Force Office of Scientific Research under Grant AFOSR-89-0296 and by the University of Kansas Structural Engineering and Materials Laboratory. Specimens were imaged with a Philips 515 scanning electron microscope using an ELMDAS image acquisition system.

References

1. A. Maher and D. Darwin, *CRINC Report* SL-76-02, Univ. of Kansas Center for Res., Lawrence, Kansas (1976).
2. A. Maher and D. Darwin, *Proc* ., 1st Intl. Conf. on Matl. Modeling, St. Louis, Missouri, III, 1705 (1977).
3. E. K. Attiogbe and D. Darwin, *SM Report* No. 16, Univ. of Kansas Center for Res., Lawrence, Kansas (1985).
4. E. K. Attiogbe and D. Darwin, *J. Engrg Mech.*, ASCE 113, 984 (1987).
5. E. K. Attiogbe and D. Darwin, *ACI Matls. J.* 84, 491 (1987).
6. E. K. Attiogbe and D. Darwin, *ACI Matls. J.* 85, 3 (1988).
7. D. Darwin and G. R. Dewey, *Cracking and Damage-Strain Localization and Size Effect*, p. 65, Elsevier Applied Science Publ. Ltd., London and New York, 1989.
8. D. Darwin, H. Zhao, G. R. Dewey, and J. L. Martin, *Micromechanics of Failure of Quasi-Brittle Materials*, p. 62, Elsevier Applied Science Publ. Ltd., London and New York, 1990.
9. D. Darwin, K. W. Ketcham, F. A. Romero, and S. Gong, *Proc.*, ASCE Engrg. Mech. Specialty Conf., Columbus, Ohio, 2, 1082 (1991).
10. D. Darwin, K. W. Ketcham, F. A. Romero, and J. L. Martin, *Proc,*. ASCE Engrg. Mech. Conf., College Station, Texas, 494 (1992).
11. K. W. Ketcham, F. A. Romero, D. Darwin, S. Gong, M. N. Abou-Zeid, and J. L. Martin, *SM Report* No. 34, Univ. of Kansas Center for Res., Lawrence, Kansas (1993).
12. K. L. Scrivener, K. D. Baldie, Y. Halse, and P. L. Pratt, *Mat. Res. Soc. Symp. Proc.* 42, 40 (1985).
13. K. L. Scrivener, and E. M. Gartner, *Mat. Res. Soc. Symp. Proc.* 114 77 (1988).
14. K. L. Scrivener, *Mat. Res. Soc. Symp. Proc.* 137 129 (1989).
15. H. Zhao and D. Darwin, *SM Report* No. 24, Univ. of Kansas Center for Res., Lawrence, Kansas (1990).
16. H. Zhao and D. Darwin, *Cem. Concr. Res.* 22, 695 (1992).
17. H. Zhao and D. Darwin, *Cem. Concr. Res.* 23, 754 (1993).
18. H. Zhao and D. Darwin, *Cem. Concr. Res.* 24, 187 (1994).
19. D. E. Newbury, D. C. Joy, P. Echlin, C. E. Fiori, and J. I. Goldstein, *Advanced Scanning Electron Microscopy and X-Ray Microanalysis*, Plenum Press, New York and London, 1986.
20. J. C. Russ, *The Image Processing Handbook*, CRC Press, Boca Raton, Florida, 1992.
21. J. I. Goldstein, D. E. Newbury, P. Echlin, D. C. Joy, A. D. Ronnig, C. E. Lyman, C. Fiori, and E. Lifshin, *Scanning Electron Microscopy and X-Ray Microanalysis*, 2nd Ed. Plenum Press, New York and London, 1992.
22. H. F. W. Taylor, *Cement Chemistry*, p. 204, Academic Press, Inc., San Diego, 1990.